**Andrew J. Provenza**
NASA Glenn Research Center,
Cleveland, OH 44135-3191
e-mail: andrew.j.provenza@nasa.gov

**Gerald T. Montague**
Army Research Lab,
NASA Glenn Research Center,
Cleveland, OH 44135
e-mail: gerald.t.montague@nasa.gov

**Mark J. Jansen**
University of Toledo,
Toledo, OH
e-mail: mark.j.jansen@nasa.gov

**Alan B. Palazzolo**
Department of Mechanical Engineering,
Texas A&M University,
College Station, TX
e-mail: a-palazzolo@tamu.edu

**Ralph H. Jansen**
University of Toledo,
Toledo, OH
e-mail: ralph.h.jansen@nasa.gov

# High Temperature Characterization of a Radial Magnetic Bearing for Turbomachinery

*Open loop, experimental force and power measurements of a radial, redundant-axis, magnetic bearing at temperatures to 1000°F (538°C) and rotor speeds to 15,000 rpm along with theoretical temperature and force models are presented in this paper. The experimentally measured force produced by a single C-core circuit using 22A was 600 lb (2.67 kN) at room temperature and 380 lb (1.69 kN) at 538°C. These values were compared with force predictions based on a one-dimensional magnetic circuit analysis and a thermal analysis of gap growth as a function of temperature. The analysis showed that the reduction of force at high temperature is mostly due to an increase in radial gap due to test conditions, rather than to reduced core permeability. Tests under rotating conditions showed that rotor speed has a negligible effect on the bearing's static force capacity. One C-core required approximately 340 W of power to generate 190 lb (845 N) of magnetic force at 538°C, however the magnetic air gap was much larger than at room temperature. The data presented are after bearing operation for eleven total hours at 538°C and six thermal cycles.* [DOI: 10.1115/1.1807413]

## Introduction

The gas turbine industry has a continued vested interest in improving engine performance and reducing net operating and maintenance costs. These goals are being realized because of advancements in materials, aeroelasticity & CFD analysis, and engine simulation. These advancements also aid in increasing engine thrust-to-weight ratios, pressure ratios, specific fuel consumption, and overall reliability through higher-efficiency engine operation at higher rotational speeds and temperatures.

Rolling element bearings and squeeze film dampers are currently used to support gas turbine engine rotors. These types of bearings are limited in temperature (<260°C) and speed (<2.5 million DN) and require both cooling air and a lubrication system. Rolling element bearings in gas turbines have been pushed to their limits and new bearing technologies must be developed to take full advantage of other aforementioned advancements.

Magnetic bearings are well suited to operate at elevated temperature, higher rotational speeds, and extreme altitudes (thin air atmosphere) and are a promising solution to current limitations.

Magnetic bearings in gas turbine engines would eliminate lubrication analysis, leaks, spills, contamination, and unnecessary maintenance due to faulty chip detection. The magnetic bearing could also provide health monitoring and adapt the rotor support to actively respond to transients such as hard aircraft landings and sudden imbalances. Magnetic bearings will enable engine designers to take full advantage of other technological advancements in turbine engine components by allowing rotor components to spin at higher speeds and at higher temperatures. As a result, turbine and compressor spools can be designed with higher operating temperatures and with significantly larger, faster, stiffer, highly damped rotors.

Contributed by the International Gas Turbine Institute (IGTI) of THE AMERICAN SOCIETY OF MECHANICAL ENGINEERS for publication in the ASME JOURNAL OF ENGINEERING FOR GAS TURBINES AND POWER. Paper presented at the International Gas Turbine and Aeroengine Congress and Exhibition, Atlanta, GA, June 16–19, 2003, Paper No. 2003-GT-38870. Manuscript received by IGTI, October 2002, final revision, March 2003. Associate Editor: H. R. Simmons.

## Literature Search

Magnetic bearing technology is being developed worldwide and is considered an enabling technology for new, hotter engine designs. There are several institutions which have been developing hardware for this high temperature application. Xu, Wang, and Schweitzer demonstrated 1 degree-of-freedom (DOF) levitation of a plate at 560°C and presented a design of a magnetic bearing system for 5 DOF in Ref. [1]. Vibration results for a blower used to recycle 700°C cathode gas, fully suspended by magnetic bearings operating at 400°C, was presented by Ohsawa et al. [2] Mekhiche et al. developed a high temperature magnetic bearing system that is described from design through room temperature testing in Refs. [3,4]. Field et al. described a complete, reliable magnetic bearing system targeted for high temperature application in Refs. [5,6]. Only in Ref. [2] can actual experimental data describing high temperature operation be found. But the data describe the vibration response of the suspended rotor at temperature. They do not present an assessment of the effects of temperature on magnetic bearing properties and system requirements.

High temperature magnetic properties of candidate magnetic materials were investigated in the 1960s by Kueser et al. [7], and recently by Kondoleon and Kelleher [8] and Fingers [9]. Hyperco 50 data in Ref. [7] does not indicate a significant decrease in permeability or saturation flux density at 538°C.

After reviewing the available literature, the authors believe that this paper provides the first baseline industry performance characteristics for actual magnetic bearing hardware during operation at temperatures up to 538°C.

The third generation high temperature, high load magnetic bearing, developed at the NASA Glenn Research Center, was first characterized at room temperature (RT) up to 20,000 rpm. It is capable of producing over 1000 lb (4.5 kN) of force per magnetic axis at RT and at speed. RT data for this bearing is presented in Ref. [10].

Data presented in this paper characterizes the third generation bearing at temperatures up to 538°C. Bearing force as a function of current, temperature, and speed to 15,000 rpm is shown. Bear-

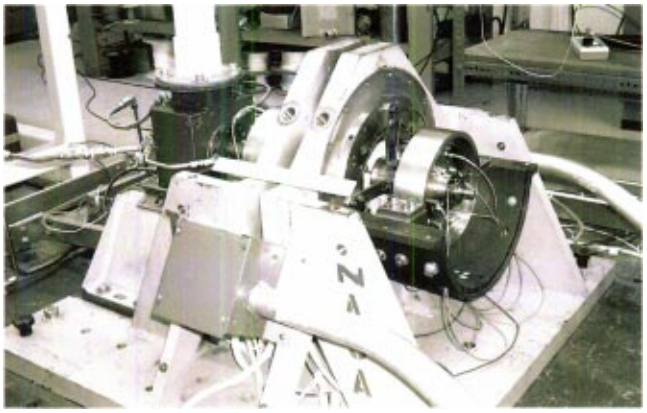

**Fig. 1 High-temperature magnetic bearing test facility at NASA Glenn Research Center**

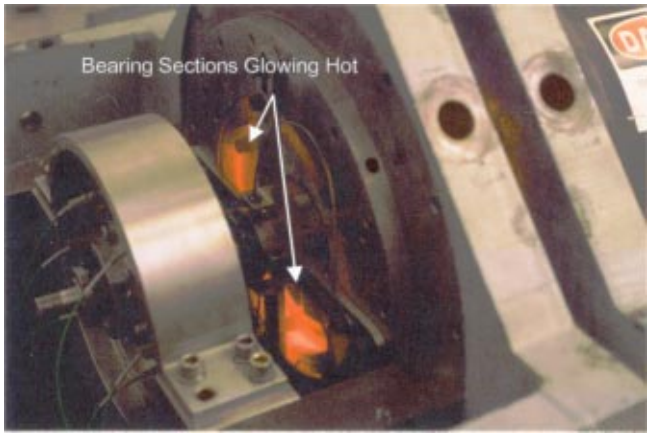


**Fig. 3 Magnetic bearing at 538°C (1000°F)**

ing power consumption measurements taken at several applied currents and temperatures are also presented. And finally, results of a simple analytical model are compared to the experimental force results.

## Test Facility

**Facility Description.** The high temperature magnetic bearing test facility is shown in Fig. 1. The structural support can accommodate thrust and radial bearings up to 22.8 cm diameter with a maximum axial loading of 22 kN and a maximum radial loading of 11.1 kN. The test facility has been configured a number of different ways [10,11].

The current configuration can be seen in Fig. 2. The magnetic bearing is located at the center of gravity of the 75-mm-diam rotor that weighs 8 kg. The 200-mm-diam stator weighs 23 kg. A 0.56 mm radial air gap exists between the stator poles and the rotor at RT. The rotor has interchangeable sleeves on each end that interface it with the support bearings, which, for these tests, are high-speed, grease packed, duplex ball bearings. For this configuration, the rotor was fitted with negative clearance sleeves so it was supported on pre-loaded ball bearings at both ends. This was done so that forces exerted by the magnetic bearing could be easily and directly measured outside the hot section at the support bearing locations. The outboard sleeve can be replaced with a positive clearance sleeve so that the magnetic bearing can support the rotor. An air turbine drives the rotor.

The magnetic bearing stator is an isolated C-core, 12-pole, heteropolar design, and is described in detail in Ref. [12]. The stator has an axial length of 76 mm. Each C-core is wrapped with two coils of 52 turns each of specially insulated and potted silver wire.

Power to the magnetic bearing is provided through tri-state, pulse width modulated (PWM) amplifiers. These components are passively filtered to remove high frequency amplifier noise that results from hard amplifier switching and for reducing EMI emissions from the bearing coils that are picked up by the eddy current position sensors.

Heat is supplied to the bearing through three, 3 kW band heaters wrapped around the stator (Fig. 2). Ground Fault Circuit Interrupts (GFCIs) have been incorporated into the heating system and the PWM amplifier circuits to protect the hardware and for safeguarding personnel. The facility is described in more detail in Ref. [12]. Figure 3 shows the facility at 538°C with the stator glowing ''orange'' hot.

**Sensors.** The facility is equipped with several different types of sensors that monitor load, temperature, rotor position, speed, and electric current.

High load, high bandwidth, piezoelectric load cells, with an accuracy of $\pm 1.5$ N, support the inboard and outboard rolling element bearings (Fig. 4). These load cells are capable of measuring loads up to 7.5 kN at 200 kHz and have a maximum operating temperature of 200°C. Two load cells are aligned along each of the three magnetic bearing axes on both support bearings for a total of 12 load cells. Each load cell was set with a preload of 1 kN. This preload value supplied symmetric structural rotor support, put the critical speed out of the operating range, and estab-

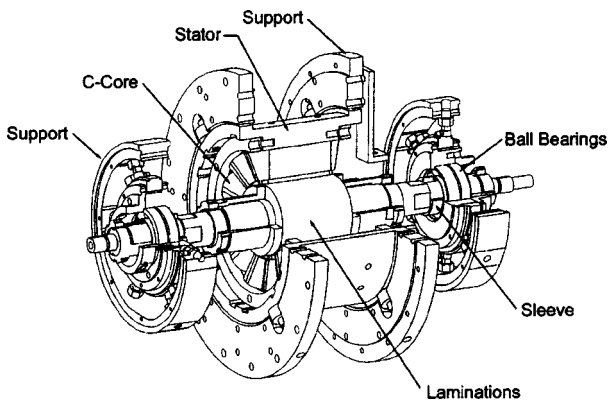


**Fig. 2 Third-generation high-temperature magnetic bearing test rig**

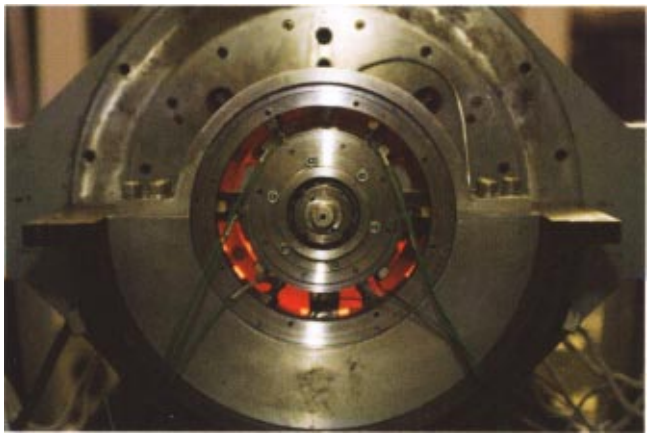

**Fig. 4 Six load cells supporting the outboard duplex ball bearing**

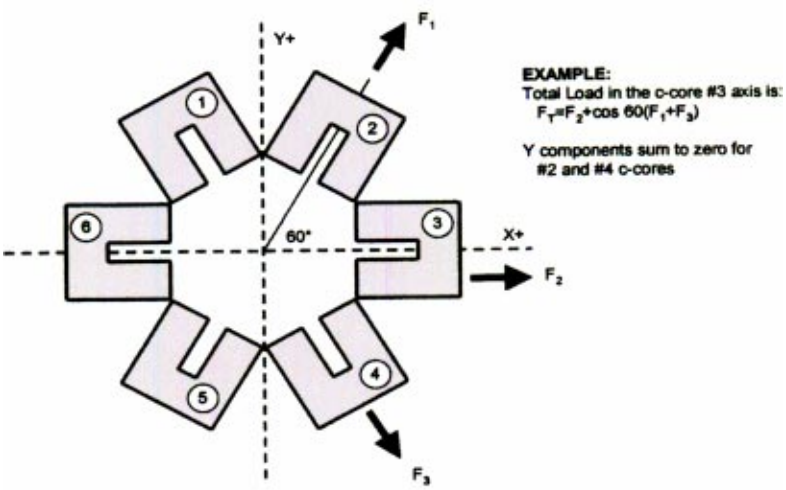


**Fig. 5 Maximum load on each magnetic axis is a vector sum of the forces from more than one C-core**

lished a large dynamic measurement range. This preload was electronically zeroed during testing and data acquisition.

Temperatures are recorded at several locations within the test rig. Both axial ends of the stator have three thermocouples mounted on them. Thermocouples are also mounted to each set of support bearings. A handheld infrared thermometer is also used periodically to gather additional thermal information about the shaft temperatures during rotation.

Commercially available, high-temperature eddy current displacement probes are used just outside the stator on both sides of the magnetic bearing to monitor rotor position. Each side has four probes $(X+, X-, Y+, Y-)$. The probes are capable of 0.0012 mm accuracy and are temperature compensated for a 538°C environment.

Other sensors include: an eddy current displacement probe used to measure rotor rpm and phase, magneto-resistive current sensors to measure C-core currents, and temperature and rpm sensors in the air turbine.

**Data Acquisition.** The facility data acquisition system is capable of capturing data at rates up to 15,000 samples per second per channel. Data are recorded for inboard and outboard bearing loads, support bearing and stator temperatures, $X$ and $Y$ axis displacements, rotor speed, and bearing C-core currents. Data are displayed in real time and can be saved directly into spreadsheet format.

## Experiment

For the tests reported in this paper, the shaft was mounted on zero clearance ball bearing supports so the load exerted by the magnetic bearing C-cores on the rotor could be measured outside of the hot section of the test facility.

The maximum load capacity for this bearing was determined by calculating the vector sum of the forces produced by any three C-cores along the middle core's centroidal axis. The primary force component is generated by the C-core inline with that axis. Each C-core adjacent to the primary C-core also contributed a component of force in the direction of the axis (Fig. 5). For example, the total load in the C-core #3 direction is the sum of the $F_2$ and the cosine of $F_1$ and $F_3$. The sine components of the $F_1$ and $F_3$ cancel each other out. This axis is referred to as the #2-3-4 magnetic axis.

**Maximum Force Produced by Single C-Core as a Function of Temperature.** Recorded data sets of load capacity versus temperature indicate the maximum load capacity of a single core and the current level where saturation begins. For these tests, C-core #1 was attached directly to a high power dc supply (100 V, 40 A) and load was measured while current was increased at five different temperatures.

Results are shown in Fig. 6. Force starts to become nonquadratic above about 12 A and saturation is almost complete at about 20 A if at lower temperatures. Saturation is less complete at higher temperatures. This suggests that forces attainable at RT can be achieved at elevated temperatures provided enough EMF can be generated to do so. Currents greater than 22 A were not applied due to concern over C-cores damage. The data also show that force production decreases by 37% at 22 A between RT and 538°C. In Ref. [11], Minihan et al. showed a similar force capacity degradation of 33% between RT and 538°C in saturation for the second generation high temperature magnetic bearing. The large decrease in load capacity for an applied current above room temperature is attributable to two causes: a minor decrease in permeability of the core material and a large increase in the radial air gap due to test conditions.

Figure 7 presents a subset of the C-core #1 data in log–log format. The top line indicates the quadratic form of the data since

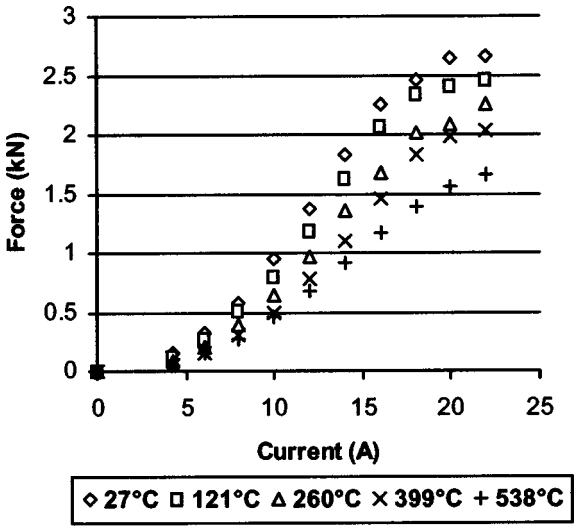


**Fig. 6 Force capacity for C-core #1 as a function of temperature**

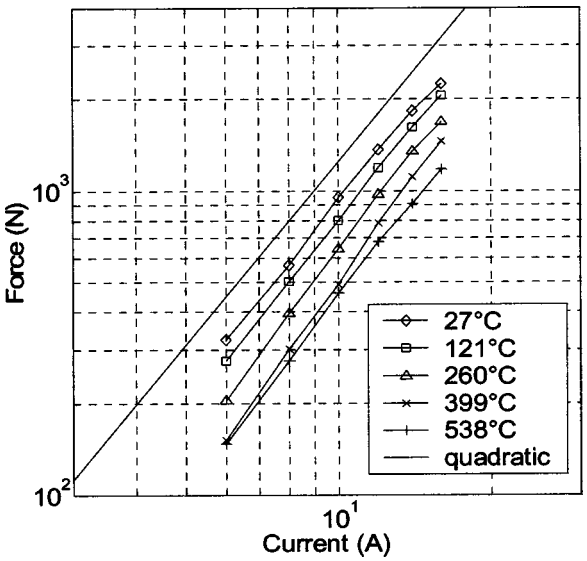


**Fig. 7 C-core #1 force data plotted on log–log plot**

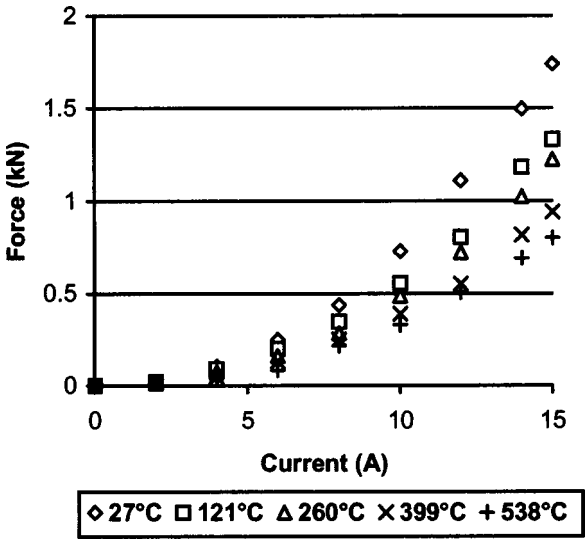


**Fig. 8 Force vs current for C-core #2 at 0 rpm**

each temperature data set is almost parallel to it. If the gap dimension was independent of temperature, then these curves would line up on top of each other. However, the actual gap dimension at each temperature can be backed out of this data using the assumption that the change in relative permeability of the core material is negligible and provided the initial gap at room temperature is known. Magnetization curves for 0.1 mm laminations of Hiperco 50 alloy in Ref. [7] do not appear to indicate an appreciable change with temperature (RT to 538°C) in relative permeability or induction for a fixed magnetizing force.

An inherent increase in gap length exists based solely upon the fact that the magnetic bearing lamination stacks are heating up. If the change in temperature of both the rotor and the stator is uniform, the gap grows by 0.5% at 538°C. One way to see this increase is to imagine replacing the air in the gap with lamination material. After applying heat, not only due the rotor and stator stacks expand, but so too does the gap material. Since this imaginary gap stack does not affect the growth of either the stator or the rotor stack, it can be concluded that the gap grows with temperature by a small amount as does the other metal components.

The coefficient of thermal expansion for Hyperco 50 is $5.28 \times 10^{-6}$ in./(in. °F) and the gap is 0.022 in. An increase of 538°C thus results in a 0.5% increase in gap length, which results in a 1% loss in force capacity.

**Individual C-Core Force Capacity as a Function of Speed and Temperature.** Typical load capacity of a single C-core as a function of current, temperature, and speed is presented here. C-core #2 load capacity data at 0 and 15,000 rpm from 27 to 538°C is shown in Figs. 8 and 9.

The data show that speed does not have an appreciable effect on the force capacity of C-core #2 at any temperature or speed to 15,000 rpm. This same result was observed previously in Ref. [10].

Figure 10 shows just how close the data matches at 538°C. Slight variations are most likely associated with the timeliness of the measurements. Gap size affects these measurements and how long the stator took to get from RT to 538°C and how long it was there is critical. Possible nonuniform frictional forces generated within the rolling element bearings as the rotor gets hot, which are not accounted for, may also be a source of variation. Small net frictional forces in the direction of load could develop if the preloads are not perfectly balanced, or if the concentricity between the rotor and the outboard rolling element bearing changes. However, the ball bearings do provide a good load path from the rotating shaft and this effect seems minimal.

The option of measuring forces directly at the stator (Fig. 11) has been tried, with difficulty, prior to this publication. The main problem was that the load cells had to be in line with the stator mechanical support and an external actuator system was required. This support configuration permitted unwanted stator deflection and position slip during dynamic tests.

As the speed increases, rotor eddy current and hysteresis losses increase. However, these losses do not affect the static load production capability of this bearing at elevated temperatures to 15,000 rpm. These losses still have negative effects on actuator bandwidth.

For this particular C-core, a decrease in load capacity of 53% is evident at 15 A between RT and 538°C. This is considerably higher than previous results have shown. Since force is proportional to the inverse square of the total air gap, small changes in air gap can greatly affect bearing output for any current values. It would appear that Figs. 8 and 9 would have shown a more favorable result if data from C-core #1 was recorded. However, it is highly unlikely that the test rig reached an equilibrium temperature when Fig. 6 data were recorded.

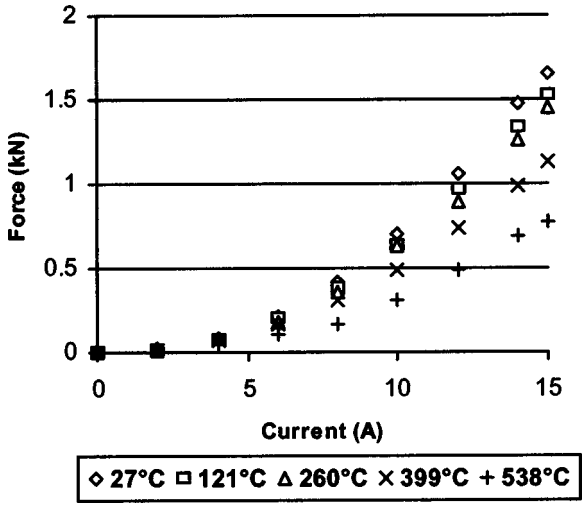


**Fig. 9 Force vs current for C-core #2 at 15,000 rpm**

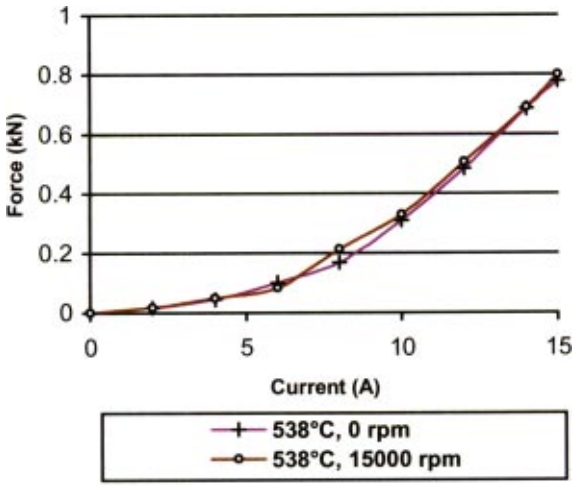


**Fig. 10 Force versus current and speed at 538°C**

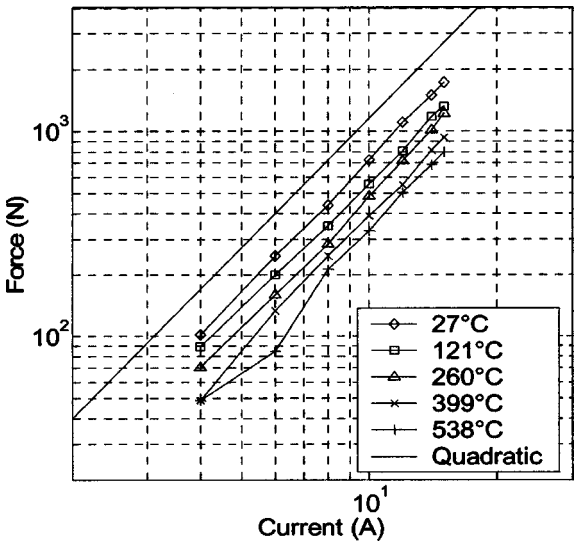


**Fig. 12 C-core #2 data at 0 rpm plotted on log–log plot**

C-core #2 tests were performed immediately when the stator had reached the desired temperature. Band heaters heat the back iron of the stator and the heat travels to all other components primarily through conduction and radiation. Consequently, the rotor takes longer to heat and therefore the air gap is larger than at room temperature. In fact, air gap size is a direct function of rotational speed, *and* the difference in temperature between the rotor and the stator.

Maintaining a constant uniform gap dimension for these tests is difficult. Concentricity within the rig has also been a challenge. The eight displacement sensors monitored *rotor* position during all the tests to ensure the rotor did not bow or change position relative to the support stand. However, the stator was not monitored, and its position may have changed slightly due to slipping, thus changing the air gap between the coils.

Figure 12 presents C-core #2 data in log–log format. The data are similar to that shown for core #1. Table 1 shows the % reduction in force and the % increase in gap for C-core #1 and #2 as a function of temperature. Force reductions were found by dividing each data set by the room temperature result. The increase in gap is directly proportional to the inverse square root of force.

**Force Capacity of an Axis as a Function of Speed and Temperature.** The previous tests were expanded upon to determine the load capacity for an axis under the condition where three adjacent C-cores all carry the same current and the opposing C-core coils carry none. The maximum load of an axis is a function of three adjacent C-cores. The two C-cores on either side of the main axis have a contribution to the total load in that axis (Fig. 5). Acting at an angle of 60 deg to the axis, these side C-cores contribute as much of the total force as the central C-core. The results of load versus current and temperature for 0 and 15,000 rpm using magnetic axis 2-3-4 are shown in Figs. 13 and 14.

Once again speed does not have an appreciable effect on the load capacity along an axis at any temperature—at least to 15,000 rpm.

To confirm that the applied magnetic force was in the same direction as the center C-core of that axis, the angle of the applied load was monitored. This was done by taking the load cell data in real-time and plotting the load vector direction versus true horizontal. The stator load angles matched the theoretical values (i.e., 0° for the #2-3-4 axis) to within a few degrees.

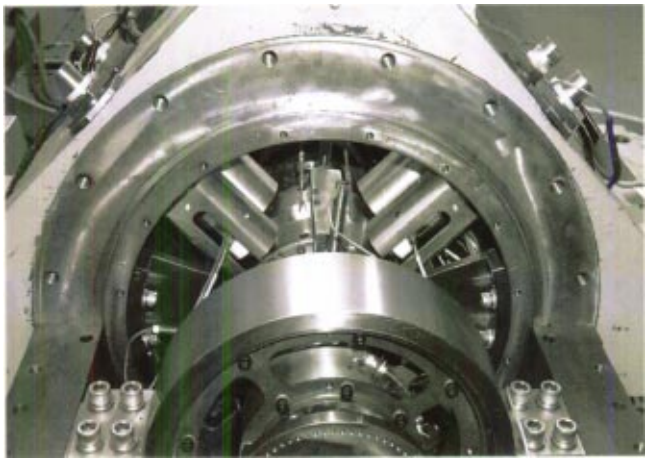

**Fig. 11 Load measurements at the stator using piezoelectric actuators**

## Power Characterization

**Power Consumption of Single Core.** The power required by the bearing C-cores as a function of magnetic force, current, temperature, and speed was also determined. At RT, the average resistance ($R$) for a C-core (2 coils) is 0.48 Ω and inductance ($L$) is 18 mH. The real power used by the C-core is a function of the output voltage of the pulse width modulation amplifier (22 kHz switching frequency) and the instantaneous current. Figure 15 shows the typical power system for one C-core.

The high switching frequency (22 kHz) of the PWM amplifier makes it difficult to measure the power required to produce bearing forces. Normal 60 Hz rms power measurement equipment cannot be used. An isolated, high impedance digital oscilloscope capable of acquiring data at one million samples per second was used to record the instantaneous voltage across the C-core coils as

**Table 1 Percent reduction in force and increase in gap as a function of temperature**

| | C-core #1 | | C-core #2 | |
|---|---|---|---|---|
| Temp (°C) | % force reduction | % gap increase | % force reduction | % gap increase |
| 121 | 13 | 7 | 21 | 13 |
| 260 | 30 | 20 | 33 | 22 |
| 399 | 44 | 34 | 47 | 37 |
| 538 | 51 | 43 | 55 | 49 |

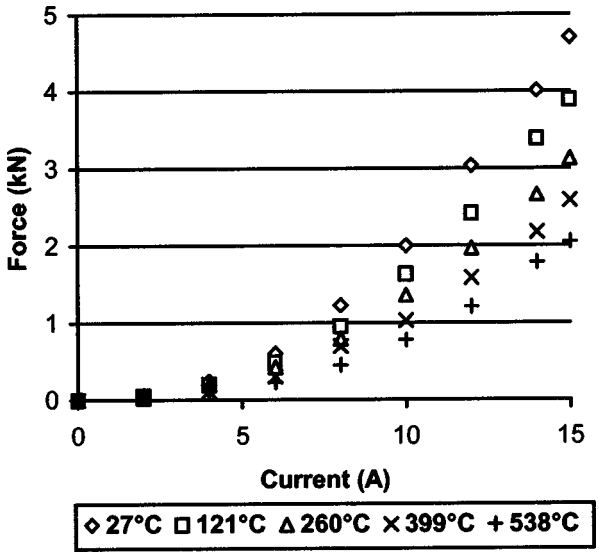


**Fig. 13 Force as a function of current and temperature for the #2-3-4 magnetic axes at 0 rpm**

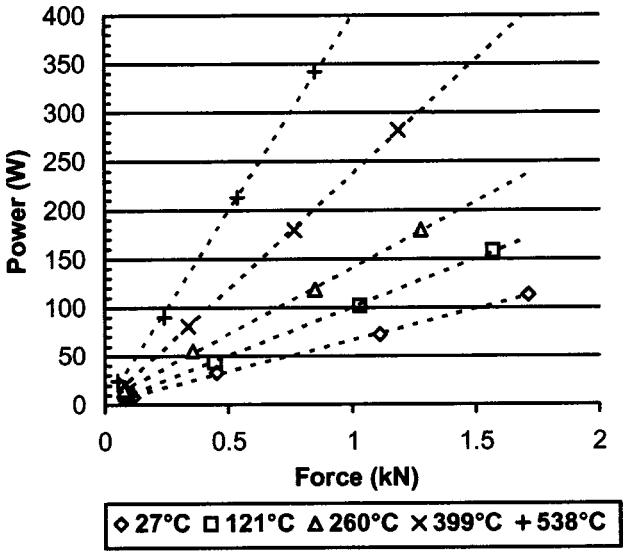


**Fig. 16 Power consumption of C-core #2 at 0 rpm**

well as the instantaneous current through the coils. Average power for each data point was calculated using a power factor equal to one.

**Full Axis Power Consumption.** Average power as a function of temperature was calculated for C-core #2 and the #2-3-4 magnetic axis at 0 rpm. The power for the magnetic axis is the sum of the power from the three C-cores in that axis. All the power calculations are shown in Figs. 16 and 17.

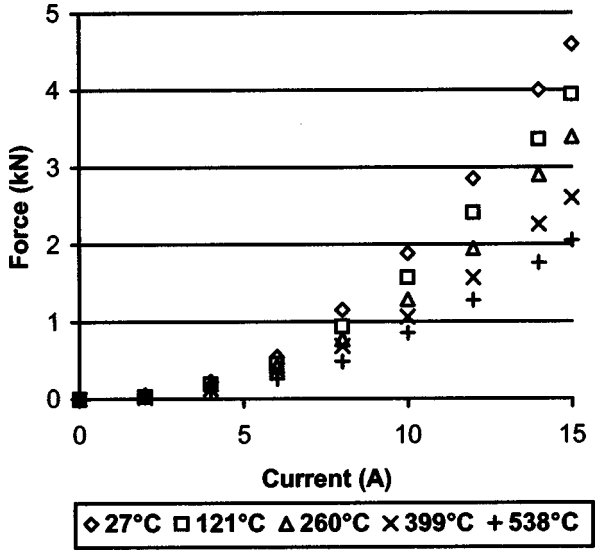


**Fig. 14 Force as a function of current and temperature for the #2-3-4 magnetic axes at 15,000 rpm**

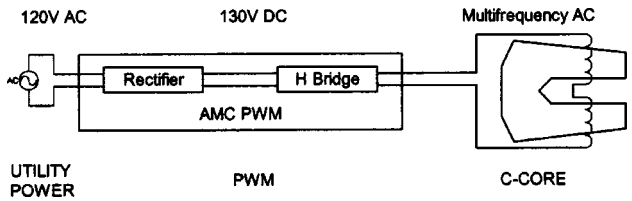


**Fig. 15 Power system for one C-core**

The largest power requirement was about 1 kW at 538°C to produce 2.3 kN on an axis. Power required to produce a specified load increases dramatically with temperature for several reasons. Resistive power loss increases since coil resistance increases. In fact, at 538°C, the resistance of the coils has increased by a factor of 3, thus required power will be at least three times as much based on this result alone. Slight degradation of the flux carrying capacity of the magnetic laminations also contributes to an increase. The other component here stems from an increase in gap dimension.

## Thermal Analysis

**Increase in Gap due to Thermal Expansion.** A major contributor to the decrease in load and the increase in power as temperature rises is the expanding gap between the rotor and the stator. Since the heaters are mounted directly on the outside of the stator, the stator heats up at a much higher rate then the rotor,

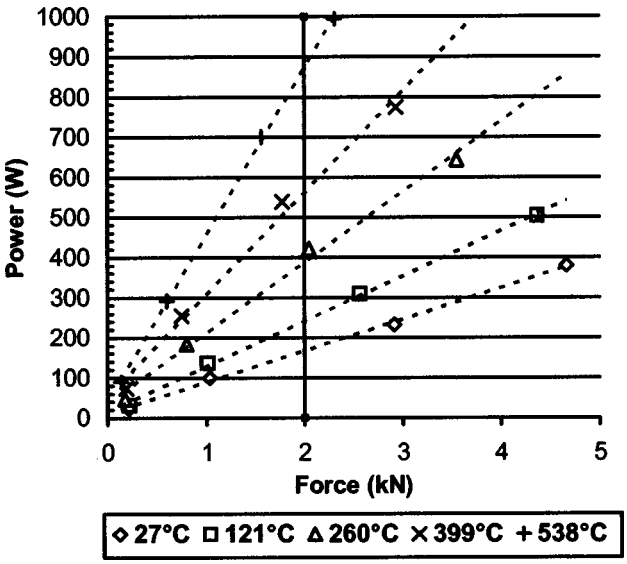


**Fig. 17 Power consumption of magnetic axis #2-3-4 at 0 rpm**

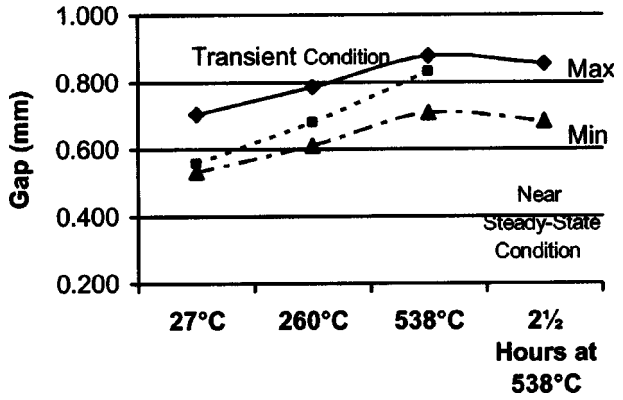


**Fig. 18 Theoretical gap between stator and rotor as a function of temperature using linear method**

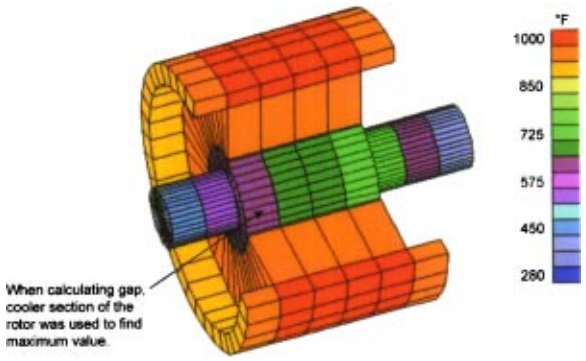


**Fig. 19 Thermal map (not FEA) of rotor and stator when rig first reaches 538°C**

which relies only on convection and radiation for heating. Thus, the rotor will not have expanded as much as the stator, and as a result, the gap will be larger than nominal.

In hindsight, it would seem advantageous to heat the rotor as well as the stator to alleviate thermal mismatch problems. With the current rig setup, however, this is not possible. Stresses generated from thermal expansion of the zero clearance bearing sleeves might cause the ball bearings to seize up. In addition, the grease used to lubricate these bearings is only rated to 135°C. In a future build, the ball bearings will be replaced with high temperature hydrostatic bearings to allow consideration of other heating methods. The hydrostatic bearings will also allow for continuous testing at higher speeds. Currently, the ball bearings heat up within minutes to their temperature limit in tests performed at high speed.

Constant gap dimension is important in the determination of force capacity and bearing power requirements, but the gap in a real engine application will not stay constant and could vary with time and external environmental conditions, such as inlet air temperature.

In order to better understand the growth of the gap, a linear thermal expansion analysis was conducted. The gap at any temperature has a minimum and maximum value just due to the tolerance stack up of the rotor and stator bearing components. The actual gap, which is somewhere between the max and min, will change with thermal mismatch. Thermal maps of the magnetic bearing section of the rotor were constructed using temperatures measured at several different points on the rig using a handheld infrared thermometer. Figure 18 shows that even after 2.5 h, the average gap dimension is greater than it is at room temperature. It is quite possible, that the rotor would never reach 538°C using the current heating method. The initial gap value for C-core #2 was determined using plastic shims to be approximately 0.56 mm. Using this reference and the values in Table 1, the actual gap can be determined. Values based on experiment and plotted in Fig. 18, fall between the max and min curves and thus provide confidence in the model.

The thermal map in Fig. 19 shows a temperature gradient on the rotor. This gradient was due to different heating rates of each of the three band heaters and also because the outer containment shell was removed for these tests allowing for convective cooling. The coolest rotor section is about 315°F. Figure 20 shows that the rotor did reach a uniform temperature of about 415°C after 2.5 h of steady heating after the stator poles reached 538°C.

In this model, the average radial gap at room temperature was 0.620 mm at 27°C. This gap increases to 0.792 mm at 538°C (Fig. 18). Since the magnetic force is a function of the inverse square of the gap distance (if core material is far from saturation), it is clear why the force at elevated temperature severely drops for a fixed supply current.

**Force Prediction.** A simple analytical prediction of force, made to verify the experimental results, is presented here. For a general magnetic actuator, the force produced by the magnetic flux in one air gap of area $A_g$ is

$$F = \frac{1}{2}\alpha\mu_0 A_g \left[\frac{NI}{2G + \frac{L_{\text{iron}}}{\mu_r}}\right]^2. \quad (1)$$

In this equation, $\mu_0$ is the magnetic permeability of free space and $NI$ is the ampere-turns of the coil(s) driving flux through the circuit. $2G$ represents the total effective magnetic air gap and $\alpha$ is a force de-rating factor, which accounts for leakage, fringing, and non-uniformity in flux density across the pole face [13]. $L_{\text{iron}}$ represents the average iron path component of the C-core circuit, and $u_r$ is the relative permeability of the iron laminations.

The actuator measurements in this paper are based on the performance of a complete C-core circuit. Each of the two C-core poles is 15° off-axis, therefore, the forced produced by a single C-core is 1.93 times that obtained using Eq. (1). Force predictions were made using the following parameters: $\alpha = 0.8$, $\mu_0 = 4\pi \times 10^{-7}$ N/A$^2$, N=52×2 turns, $A_g = 12.9$ cm$^2$, $G_0 = 0.559$ mm, $L_{\text{iron}} = 145$ mm, $\mu_r = 500$. A nominal $\mu_r$ was calculated from the local slope of the Hyperco 50 data in Ref. [7] at 12 Oe and RT. 12 Oe corresponds to about 10 A in these third generation radial bearing C-cores.

Figure 21 shows a comparison between the predicted force and the measured force for C-core #1. An initial gap, $G_0$, of 0.47 mm was used in the predictions since the force in C-core #1 was considerably higher than that in C-core #2. The trend for gap increase backed out of the measured data for C-core #1 shown in Table 1 was used to determine predicted gap values in C-core #1

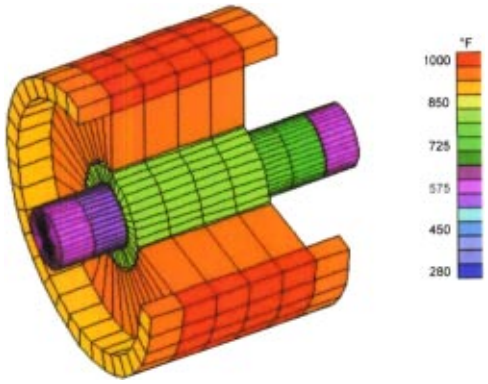


**Fig. 20 Thermal map (not FEA) of rotor and stator after rig at 538°C for 2.5 h**

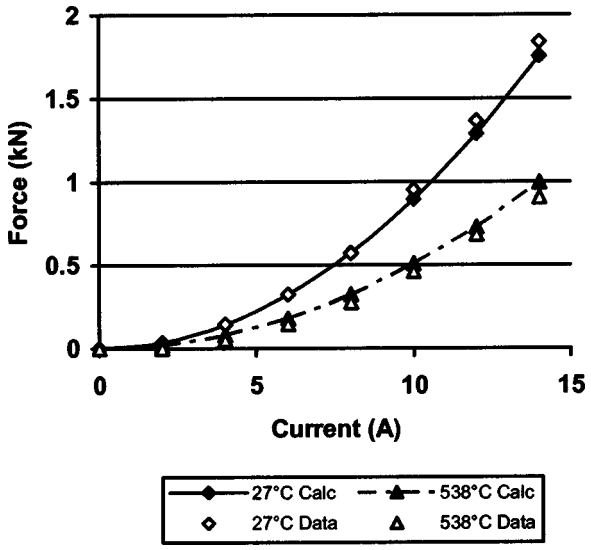


**Fig. 21 Theoretical force prediction versus actual measured values for C-core #1**

using $G_0$ as a reference. There is good agreement between the calculated load and the actual measurements when the variation in gap is considered.

It becomes quite clear that exact knowledge of the gap dimension is imperative to obtaining a detailed comparison between experimental results and analytical predictions. This measurement is not easy to obtain, however. The gap in this test rig is difficult to get at and high temperatures limit probe or shim materials.

## Concluding Remarks

Magnetic applied force and electric power for a high load, high speed, high temperature radial magnetic bearing for turbomachinery were measured. Even though the shaft is not doing any work and the rotor is not levitated, these tests provide baseline industry performance characteristics for actual hardware. Load capacity and power consumption of both a single C-core and a magnetic axis were measured from 27 to 538°C. Thermal analysis of the test rig to investigate gap growth due to non-uniform heating was performed. Theoretical force predictions were compared to actual results with good correlation. No appreciable decrease in static force production capability was observed due to rotation up to 15,000 rpm at any temperature. Future experimental work will include high temperature, high-speed levitation tests without the use of rolling element bearings and high temperature force measurements of a magnetic thrust bearing. Future analytical work will include the development of an advanced model that includes the effect of applied magnetizing force and temperature on the relative permeability of the core material as well as the effects of rotation and thermal mismatch on bearing air gap.

## Acknowledgments

This research was funded by NASA Glenn Research Center's Smart Efficient Components Program, which is managed by Robert D. Corrigan. The authors would like to thank Peter Kascak (University of Toledo) for his assistance in the power measurements, Julie Roden (Analex) for her thermal expansion analysis, John Poles (NASA Glenn) for his significant electrical contributions, and Tim Czaruk (QSS) for test support. The authors would also like to recognize Gerald Brown (NASA Glenn) and Albert Kascak (ARL at NASA Glenn) for their expert guidance and review. Final recognition is for Texas A&M students Randy Tucker, Jason Preuss, and Andrew Hunt who helped design and construct the high temperature coils used in this bearing.

## References

[1] Xu, L., Wang, L., and Schweitzer, G., 2000, "Development of Magnetic Bearings for High Temperature Suspension," *Proceedings of the 7th ISMB*.
[2] Ohsawa, M., Furuya, E., Marui, E. et al., 1998, "High Temperature Blower for a Molten Carbonate Fuel Cell Supported by Magnetic Bearings," *Proceedings of the 6th ISMB*, pp. 32–41.
[3] Mekhiche, M., Nichols, S., Oleksy, J., Young, J., Kiley, J., and Havenhill, D., 2000, "50K RPM, 1100°F Magnetic Bearings for Jet Turbine Engines," *Proceedings of the 7th ISMB*.
[4] Mekhiche, M., Nichols, S., Hevenhill, D. et al., 2000, "High-Speed, High-Temperature Magnetic Bearings for Jet Turbine Engine Application," *Proceedings of the International Conference on Electrical Machines* (ICEM).
[5] Field, R. J., and Iannello, V., 1998, "A Reliable Magnetic Bearing System for Turbomachinery," *Proceedings of the 6th ISMB*, pp. 42–51.
[6] Field, R. J., Sortore, C. K., and Iannello, V., 2000, "A Magnetic Bearing System for More-Electric Engines," Proceedings of ASME/IGTI Turbo Expo.
[7] Kueser, P. et al., 1967, "Properties of Magnetic Materials for Use in High-Temperature Space Power Systems," NASA SP-3043.
[8] Kondoleon, A., and Kelleher, W., 2000, "Soft Magnetic Alloys for High Temperature Radial Magnetic Bearings," *Proceedings of the 7th ISMB*.
[9] Fingers, R., 1999, "Creep Behavior of Thin Laminations of Iron-Cobalt Alloys for Use in Switched Reluctance Motors and Generators," AFRL-PR-WP-TR-1999-2053.
[10] Montague, G. T., Jansen, M. J., Provenza, A. P., Jansen, R. H., Ebihara, B., and Palazzolo, A., 2002, "Room Temperature Characterization of a Magnetic Bearing for Turbomachinery," NASA Tech. Memo-2002-211904.
[11] Minihan, T., Palazzolo, A., Provenza, A., Montague, G. T., and Kascak, A. F., 2002, "Fail Safe, High Temperature Magnetic Bearings," *Proceedings of the ASME/IGTI Turbo Expo*.
[12] Jansen, R. H., Ebihara, B. E., Montague, G. T., Provenza, A. J., Jansen, M. J., Palazzolo, A., Tucker, R., Preuss, J., and Hunt, A., 2003, "Design and Fabrication of a High Temperature, Radial Magnetic Bearing for Turbomachinery," NASA Tech. Memo, 2003-212300.
[13] Knospe, C. R., and Maslen, E. H., 1999, "Introduction to Active Magnetic Bearings," University of Virginia Short Course.